Structure-dependent anisotropy of the photoinduced optical nonlinearity in calcium doped ZnO nanorods grown by low cost hydrothermal method for photonic device applications

B. Santoshkumar [a], S. Kalyanaraman [a, *], R. Vettumperumal [b], R. Thangavel [c], I.V. Kityk [d], S. Velumani [e]

[a] PG and Research Dept. of Physics, Sri Paramakalyani College, Alwarkurichi, 627 412, India
[b] Dept. of Physics, V.V. College of Engineering, Tisaiyanvilai, Tirunelveli, 627 657, India
[c] Dept. of Applied Physics, Indian School of Mines, Dhanbad, 826 004, India
[d] Electrical Engineering Dept., Czestochowa University Technology, Czestochowa, Poland
[e] Dept. of Electrical Engineering (SEES), CINVESTAV-IPN, Av. Instituto Politecnico Nacional, # 2508, Col. San Pedro Zacatenc 07360, Mexico D.F, Mexico

ARTICLE INFO

ABSTRACT

Calcium doped zinc oxide nanorods on ZnO seed layers were grown by hydrothermal method. Photo-induced bicolour laser treatment was done on the samples and the effective second order nonlinear coefficient (d_{eff}) has been measured. The morphology of the samples was investigated by the field emission scanning electron microscope (FESEM) images. The structural parameters acquired from X-ray diffraction (XRD) patterns have been correlated with the measured d_{eff}. The results have revealed that 15 mol% Ca doped ZnO nanorod showed maximum d_{eff} because of the Lorentz local field established along the length of the nanorod. The aspect ratio and stress play a significant role in enhancement of d_{eff}. The nonlinearity has been correlated with the absorption cross sections.

1. Introduction

Zinc oxide (ZnO) is the most attractive and widely studied material in the past two decades or so because it finds application in the areas of optoelectronic devices, piezoelectric devices, spintronics, lasing, solar cells and sensors [1–6]. It has excellent properties like high electron mobility, high thermal conductivity, high transparency, wide and direct bandgap (3.37 eV), large exciton binding energy (60 meV) at room temperature etc. ZnO can be grown in nanostructure form easily. It can be grown by numerous methods such as sputtering [7], chemical vapour deposition (CVD) [8], pulsed laser deposition (PLD) [9], atomic layer deposition (ALD) [10] and hydrothermal method [11–19]. Among these, the hydrothermal method offers many advantages such as low cost, convenience with simple equipment, low temperature growth [14–19] etc.

In recent years the topical interest of wurtzite ZnO is its non-linear optical (NLO) properties [20–27]. The nonlinear behaviour is more for polar crystals like ZnO as the optical nonlinearity is enhanced due to the formation of the charge density non-centrosymmetry and creation of dipole–dipole interaction between the atoms at the surfaces. The nanomaterials of ZnO possess cost-effectiveness and high damage threshold. Among the various nanostructures of ZnO, nanorod (NR) is one of the suitable silhouettes for NLO applications due to its well-controlled growth condition and significantly enhanced NLO responses with respect to bulk materials. The nonlinearity is due to strong polarization anisotropy and size/aspect ratio dependency on these materials [23,28]. Lorentz local field effect is responsible for the size dependent polarization anisotropy observed for them [23–25,28]. Photoinduced nonlinear optical effects in ZnO films [29,30], with Au nanoparticle deposition [31], by doping rare earths like Nd [32], Er [33] etc., have been studied earlier.

There are plenty of higher order NLO materials like ZnO. Especially with respect to second order nonlinearity, ZnO finds its applications in frequency converters in laser sources at new

wavelengths, electro-optic switching, as modulators in telecommunication etc. These types of materials combined with inexpensive diode lasers can be used for generating optical frequencies over a broad range [34]. Second order nonlinearity could be tuned by controlling the length, diameter and ordering degree of the cost effective nanorods. Since we deal with the nanorods, it is possible to evaluate only the effective second order susceptibility and definition of the particular tensor components is not possible for these materials because they are not in the form of single crystals. For determining the frequency conversion efficiency, gain and threshold for optical parametric devices, the effective second order nonlinear coefficient (d_{eff}) plays an important role [35]. This parameter d_{eff} defines effective transformation of the laser light to the doubling of frequency. Knowing this parameter we can do direct changes in order to improve the important technological parameters like efficiency of the fundamental laser beam from 1064 nm to the doubled frequency 532 nm of green signal which is important for the laser frequency modulators. Additionally these materials may be used for visible control of IR laser light of 1064 nm.

In our present study, after doping calcium in ZnO nanorod by low cost hydrothermal method, the important second order nonlinear parameter, the effective second order nonlinear coefficient (d_{eff}) was measured using photoinduced bicolour laser treatment at 1064 and 532 nm. We correlated the structural parameters like stress, dimensions of the nanorod etc., with the witnessed d_{eff} values in p-polarized geometry of the beam based on the Lorentz local field.

2. Materials and methods

The soda lime glass substrates were cleaned by an ultrasonic cleaner with aqua regia (HNO_3:HCl in 1:3 ratio), acetone, ethanol for each 20 min, then cleaned with deionized water and dried. Before hydrothermal deposition, the normal glass substrates were spin coated with ZnO seed layer which was prepared by sol–gel synthesis. The preparation of ZnO seed layers was given elsewhere [36,37]. For preparing nanorod, calcium is doped with ZnO by taking zinc nitrate hexahydrate ($Zn(NO_3)_2 \cdot 6H_2O$), calcium chloride dihydrate ($CaCl_2.2H_2O$) and hexamethylene tetramine (HMT, $C_6H_{12}N_4$) as the precursors. Calcium was incorporated at different percentages such as 5 mol%, 10 mol%, 15 mol% and 20 mol% in the ZnO matrix. The precursor solutions of 50 mM concentration were mixed with deionised water and stirred in a beaker at room temperature for half an hour. After filtration, the seed layers were suspended inside this solution facing upside down. The beaker was covered with an aluminium foil and kept at 90 °C in a hot air oven [38]. After 4 h, it was taken out and the samples were cleaned by sonication with deionised water and dried at 100 °C for 10 min. For all these samples the photoinduced effective second order nonlinear coefficient (d_{eff}) was measured using bicolour Nd:YAG nanosecond laser at 1064 and 532 nm wavelength. The morphology was examined using the field emission scanning electron microscope (FESEM, Zeiss Supra 55). X-ray diffraction patterns were recorded using Bruker, Germany (Model: D8) X-ray diffractometer with $CuK\alpha_1$ (1.5406 Å) radiation and subsequently analysed to extract the structural parameters. The absorption spectrum was recorded with Agilent Cary 5000 UV–visible spectrophotometer.

3. Results and discussion

Fig. 1 shows the dependence of photoinduced effective second order nonlinear coefficient (d_{eff}) of calcium doped ZnO nanorods grown by hydrothermal method with the intensity of the bicolour laser beam. Douayar et al. (2013) has reported earlier about second
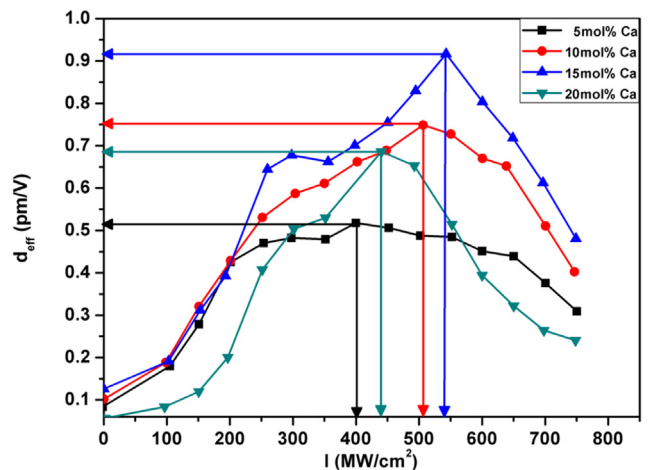

Fig. 1. Photoinduced effective second order nonlinear coefficient (d_{eff}) versus the power density during bicolour laser treatment.

harmonic generations in Tm doped ZnO measured using the bicolour Nd:YAG laser at 1064 and 532 nm wavelength. The similar measurements were performed for our samples. Optimal ratio of intensities between these two beams was equal to 5:1. Additionally a cw 12 mW He–Ne laser beam was used as a probing beam in Senarmont method to detect the photoinduced birefringence with accuracy of 10^{-6} [39]. The p-polarized beam probed the samples to witness d_{eff}. It was measured with respect to the intensity of the incident laser beam [Fig. 1]. The measured d_{eff} values were 0.51, 0.75, 0.92, 0.68 pm/V for 5 mol%, 10 mol%, 15 mol% and 20 mol% of CaZnO respectively and the maximum value is observed for 15 mol % CaZnO. When the intensity of the laser beam reaches the saturation level (I_s), the d_{eff} value is found to decrease. However a comparison with other forms of ZnO [32,40–42] indicates that the obtained second order nonlinear coefficient values are considerably higher.

In order to have a clear picture on the structure of the samples, FESEM images have been taken. Fig. 2 shows the plane-view images of all the samples. The inset images show the tilted (25°~45°) view of the nanorods and the EDX spectra which confirm the calcium doping. From the figure, it was obvious that the diameter of 15 mol% CaZnO was smaller with respect to others. The average diameters of 5 mol%, 10 mol%, 15 mol% and 20 mol% CaZnO were found to be ~275, ~193, ~92, ~147 nm respectively. The length of the nanorods varies for these samples from ~592, 712, ~670, ~488 nm. In our case the diameters are changing monotonically and hence diameter plays a vital role here. The change in dimension of the as grown Ca doped ZnO nanorod induced optical nonlinearity via dipole–dipole interaction based charge localization [43]. Here the interaction might have taken place at the surface parallel to the diameter of the nanorod and along its length. Having a larger dimension and accommodating larger number of atoms along its length, the nanorod was having higher interaction in the longitudinal axis rather than in the transverse axis because in transverse direction the dimension (diameter) of the nanorod is smaller than that is in the longitudinal direction (length). Therefore the Lorentz local field has been set up along the length of the nanorod and induces nonlinearity. This Lorentz local field overshadowed the bulk effect and the nonlinearity was superior in the nanorods along the c-axis. So in 15 mol% CaZnO the longitudinal contribution of the Lorentz field dominated the transverse contribution. From Table 1 it is evident that 15 mol% CaZnO possesses higher aspect ratio. The d_{eff} values for all the samples are having linear dependence on aspect ratio [44]. Hence
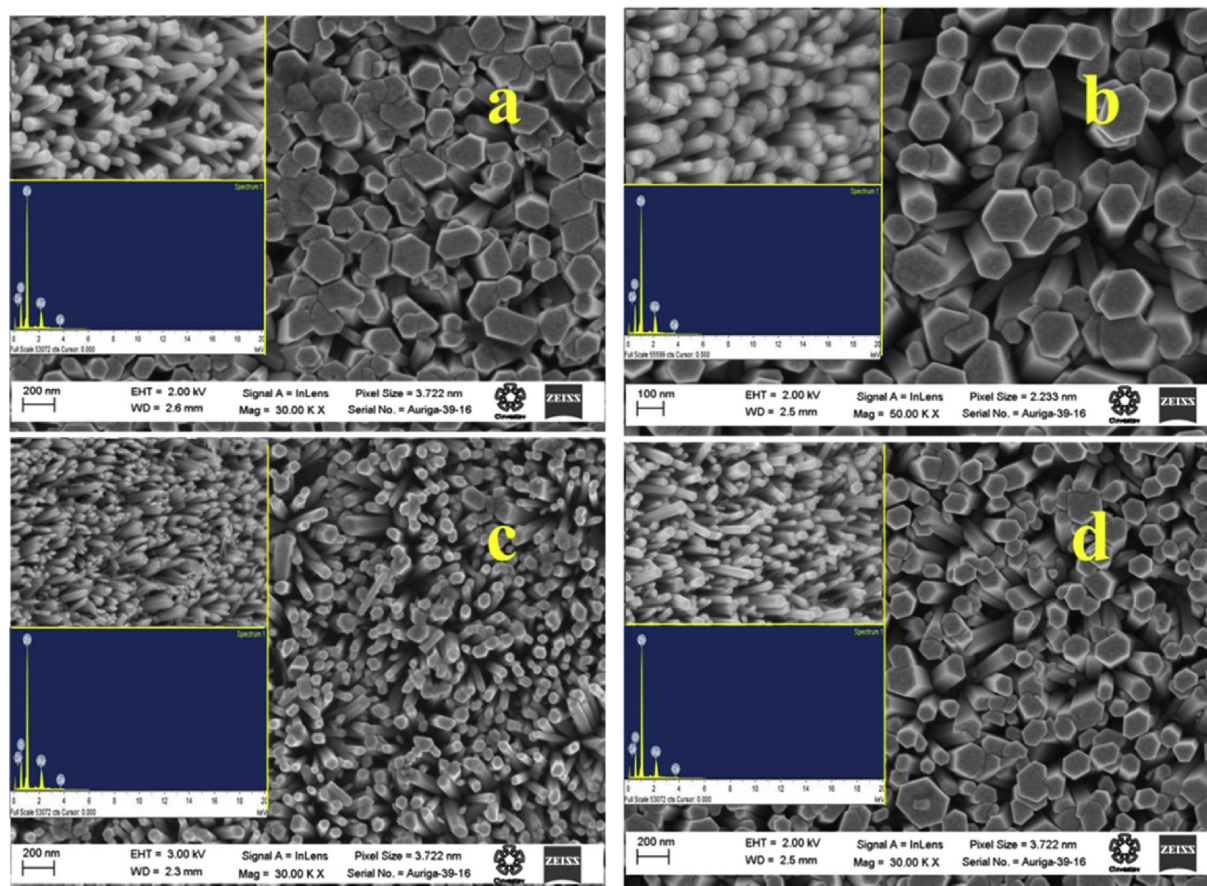
Fig. 2. FESEM images of Calcium doped ZnO nanorod samples. (a) 5 mol% (b) 10 mol% (c) 15 mol% & (d) 20 mol%. Inset shows the corresponding tilted view (25°~45°) and EDX spectra of the nanorods.

Table 1
Effective second order nonlinear coefficient (d_{eff}), Intensity of the preparation beam and aspect ratio.

Calcium doping conc. in ZnO (mol%)	d_{eff} (pm/V)	I_s (MW/cm^2)	Aspect ratio (l/a)
5	0.51	401	2.15
10	0.75	506	3.69
15	0.92	542	7.28
20	0.68	439	3.32

Table 2
Structural parameters calculated from XRD patterns.

Calcium doping conc. in ZnO (mol%)	a (Å)	c (Å)	Crystallite size D (nm)	Biaxial stress (GPa)	$TC_{(002)}$
5	3.247	5.193	46.365	−1.1675	3.5365
10	3.245	5.188	150.87	−1.5683	4.3817
15	3.250	5.206	44.85	0.0087	3.5586
20	3.251	5.210	47.41	0.3485	3.5334

Table 3
Observed optical parameters from UV–vis absorption spectrum.

Calcium doping conc. in ZnO (mol%)	Absorbance at 532 nm	Absorption coefficient (α) at 532 nm $\times 10^4$ cm^{-1}	Band gap (eV)
5	0.96	3.250	3.235
10	1.53	5.116	3.187
15	1.86	6.210	3.250
20	1.37	4.603	3.260

in p-polarized beam, which is mainly taken along c-axis, the d_{eff} value is more for the nanorod with higher aspect ratio, in our case, it is with 15 mol% CaZnO. Moreover the saturation intensity level (I_s) is also linearly depending on the aspect ratio as is evident from Table 1.

The XRD patterns of the prepared samples were shown in Fig. 3 for further investigation. They were having the same wurtzite structure consistent with the earlier reported values (JCPDS 36-1451). The high (002) peaks [inset of Fig. 3] rendered high value of texture coefficient (in Table 2) was a clear indication of c − axis
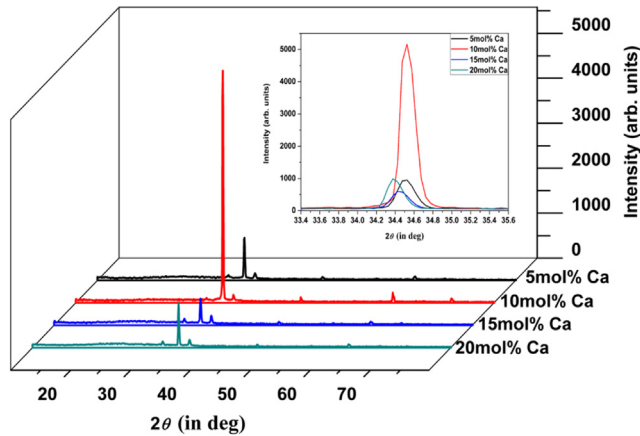
Fig. 3. XRD patterns of 5 mol%, 10 mol%, 15 mol%, 20 mol% of Ca doped ZnO nanorods. Inset shows the (002) peak profile.

oriented growth of nanorods. The interaction between the film and the substrate upon deposition caused this preferential growth. The growth along the c-axis is dominant due to the high surface energy of the (0001) plane [45]. Also there was no evidence for the formation of secondary phase upon calcium doping. The (002) peak occurs at $2\theta = 34.52°$, $34.55°$, $34.45°$, $34.40°$ for 5 mol%, 10 mol%, 15 mol% and 20 mol% CaZnO nanorods respectively. The diffraction peak was shifted to higher angle for 10 mol% CaZnO and the lattice constant c decreases since Ca gets substituted at Zn sites (ionic radii of $Zn^{2+} = 0.074$ nm and $Ca^{2+} = 0.099$ nm). For higher concentration of Ca, angle of diffraction decreases again resulting in an increase in c-lattice constant. Such an increment can be attributed to increase in interstitial Zn/Ca.

The mean crystallite sizes of the samples were calculated using Scherrer's formula [46].

$$D = \frac{0.9\lambda}{\beta cos\theta}$$

where $\lambda = 1.5406$ Å for $CuK\alpha_1$ radiation, β is the FWHM and θ is the Bragg angle.

15 mol% CaZnO has the smaller crystallite size of ~44 nm and the sizes are varied for all samples upto ~150 nm. The change in crystallite sizes upon doping was due to the change in the values of stress. The film thickness is small compared to the substrate and in addition there is lattice mismatch leading to induced stress in the nanorods. The biaxial stress was calculated [47] as:

$$\sigma = \left[\frac{2C_{13}^2 - C_{33}C_{11} - C_{33}C_{12}}{C_{13}}\right]\frac{c_0 - c}{c_0}$$

where, C_{ij} is elastic stiffness constant of ZnO, $C_{11} = 209.7$ GPa, $C_{12} = 121.1$ GPa, $C_{33} = 210.9$ GPa and $C_{13} = 105.1$ GPa.

$$\therefore \sigma = -453.6 \times 10^9 \frac{c_0 - c}{c_0}$$

As doping increases, initially the stress increases and a change in compressive stress to tensile stress occur in 15 mol% CaZnO. This sample has lesser crystallite size and having a 2θ value closer to bulk ZnO ($34.43°$ − JCPDS 36-1451), so are the lattice constants a and c. Hence this sample is having lesser biaxial stress coefficient. So one can infer that 15 mol% CaZnO is in a kind of relaxed state namely in a phase transition state (from compressive nature to tensile, as evident from the values in Table 2). Hence it can

accommodate more number of dipoles leading to the enhancement of photoinduced nonlinearity. A decrease in stress favoured the decrease in the diameter of the nanorod [48] which in turn enhances the nonlinearity. The as-grown nanorods with different diameters might be a stress-driven process. From the variation in the state of stress we could understand the mechanism for diameter control of nanorods. Lesser diameter leads to higher aspect ratio. Along with the lesser stress values, the higher aspect ratio also supports the enhancement in nonlinearity.

From UV−vis absorption spectrum [see Fig. 4], it is evident that the absorbance and absorption coefficient at 532 nm (wavelength used for bicolour treatment) are found to have the maximum value for 15 mol% CaZnO. Higher value of absorbance at the preparation beam wavelength (532 nm) plays a decisive role in the determination of the observed effective second order nonlinear coefficient. The linear absorption coefficient (α) increases with effective thickness of the sample (L_{eff}) by $L_{eff} = [1\text{-}exp(-\alpha l)]/\alpha$ [49]. Also the thickness of the sample enhances the second order nonlinearity [50]. Here 15 mol% CaZnO is having the higher α (see Table 3) which in turn has higher d_{eff} value. Hence the higher absorption coefficient enhances the nonlinearity in our samples. The band gaps of the samples have been determined by the Tauc plot [Fig. 5]. The inset of Fig. 5 shows the variation of band gap with the biaxial stress. There is a linear relation governed by the equation $E_g = 3.25802 + 0.03409\,\sigma_{xx}$ that exists between the band gap E_g and biaxial stress σ_{xx}. The possible reason for this variation might be due to the larger valence band maximum offset compared to conduction band maximum in ZnO. Also there might be a strong p-d coupling in valence band of ZnO [51].

4. Conclusion

The photoinduced effective second order nonlinear coefficient (d_{eff}) value was measured for 5 mol%, 10 mol%, 15 mol% and 20 mol% of Ca doped ZnO nanorods grown by hydrothermal method. The d_{eff} value depends not only on the aspect ratio, but also on parameters like stress coefficient, absorbance etc. These parameters were responsible for 15 mol% CaZnO to accommodate more number of atoms along the longitudinal axis rather than transverse axis leading to the formation of larger number of dipoles along c-axis compared to basal plane. This much enhanced dipoles created Lorentz local field in these directions. This Lorentz local field was found to be responsible for the dipole−dipole interaction and accounts for higher nonlinearity in these samples. So in 15 mol% CaZnO there is an enhanced bond dipole moment along (0001)
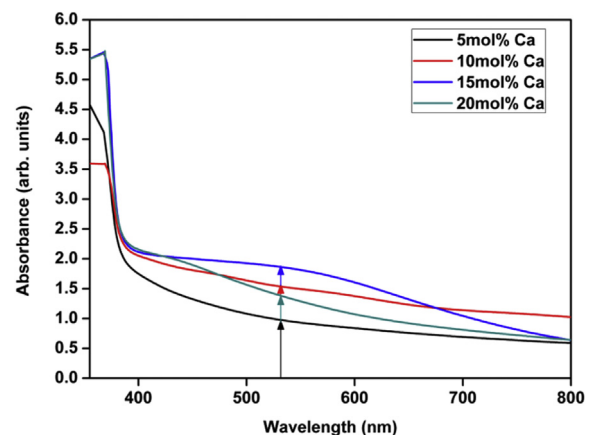

Fig. 4. UV−vis absorption spectrum of 5 mol%, 10 mol%, 15 mol%, 20 mol% of Ca doped ZnO nanorods.
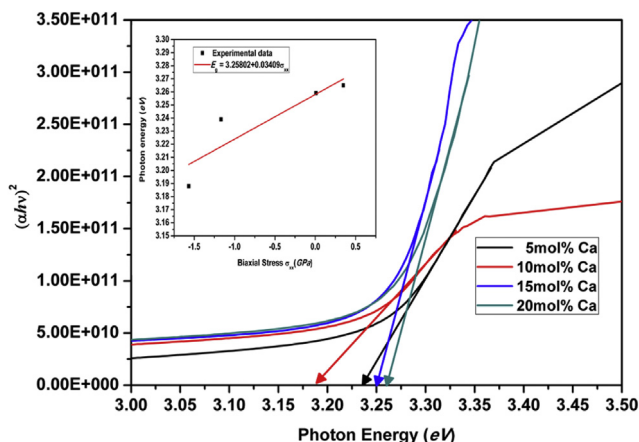
Fig. 5. Tauc plot of 5 mol%, 10 mol%, 15 mol%, 20 mol% of Ca doped ZnO nanorods. Inset shows the variation of band gap with biaxial stress.

direction and leads to the increase in observed d_{eff}. Moreover 15 mol% CaZnO was held in a state of relaxation which in turn boosted the formation of Lorentz local field. This type of highly structure-dependent anisotropies of the photoinduced second-order nonlinearity in calcium doped ZnO nanorods grown by low cost hydrothermal method has greater potential in the applications for nanolasers, high resolution photodetectors, electro-optic switching, as modulators in telecommunication etc. These types of materials combined with inexpensive diode lasers can also be used for generating optical frequencies over a broad range. Additionally these materials may be used for visible control of IR laser light of 1064 nm.

Acknowledgement

References

[1] J.X. Wang, X.W. Sun, Y. Yang, H. Huang, Y.C. Lee, O.K. Tan, L. Vayssieres, Nanotechnology 17 (2006) 4995.
[2] M.H. Huang, S. Mao, H. Feick, H.Q. Yan, Y. Wu, H. Kind, et al., Science 292 (2001) 1897.
[3] K. Keis, L. Vayssieres, S.E. Lindquist, A. Hagfeldt, Nanostruct. Mater. 12 (1999) 487.
[4] S.C. Minne, S.R. Manalis, C.F. Quate, Appl. Phys. Lett. 67 (1995) 3918.
[5] T. Shibata, K. Unno, E. Makino, Y. Ito, S. Shimada, Sens. Actuators A 102 (2002) 106.
[6] H.M. Lin, S.J. Tzeng, P.J. Hsiau, W.L. Tsai, Nanostruct. Mater. 10 (1998) 465.
[7] D.C. Kim, B.H. Kong, S.O. Jun, H.K. Cho, D.J. Park, J.Y. Lee, Thin Solid Films 516 (2008) 5562.
[8] G. Kiriakidis, M. Suchea, S. Christoulakis, P. Horvath, T. Kitsopoulos, J. Stoemenos, Thin Solid Films 515 (2007) 8577.
[9] Y. Zhao, Y.J. Jiang, Y. Fang, J. Cryst. Growth 307 (2007) 278.
[10] C.R. Kim, J.Y. Lee, C.M. Shin, J.Y. Leem, H. Ryu, J.H. Chang, H.C. Lee, C.S. Son, W.J. Lee, W.G. Jung, S.R. Tan, J.L. Zhao, X.W. Sun, Solid State Commn. 148 (2008) 395.
[11] X.Q. Zhao, C.R. Kim, J.Y. Lee, J.H. Heo, C.M. Shin, H. Ryu, J.H. Chang, H.C. Lee, C.S. Son, W.J. Lee, W.G. Jung, S.T. Tan, J.L. Zhao, X.W. Sun, Appl. Surf. Sci. 255 (2009) 4461.
[12] X.Q. Zhao, C.R. Kim, J.Y. Lee, C.M. Shin, J.H. Heo, J.Y. Leem, H. Ryu, J.H. Chang, H.C. Lee, C.S. Son, B.C. Shin, W.J. Lee, W.G. Jung, S.T. Tan, J.L. Zhao, X.W. Sun, Appl. Surf. Sci. 255 (2009) 5861.
[13] X.Q. Zhao, J.Y. Lee, C.R. Kim, J.H. Heo, C.M. Shin, J.Y. Leem, H.H. Ryu, J.H. Chang, H.C. Lee, W.G. Jung, C.S. Son, B.C. Shin, W.J. Lee, S.T. Tan, J.L. Zhao, X. Sun, Phys. E 41 (2009) 1423.
[14] T. Sahoo, S.K. Tripathy, Y.T. Yu, H.K. Ahn, D.C. Shin, I.H. Lee, Mater. Res. Bull. 43 (2008) 2060.
[15] S. Li, S. Zhou, H. Liu, Y. Hang, C. Xia, J. Xu, S. Gu, R. Zhang, Mater. Lett. 61 (2007) 30.
[16] M.N.R. Ashfold, R.P. Doherty, N.G. Ndifor-Angwafor, D.J. Riley, Y. Sun, Thin Solid Films 515 (2007) 8679.
[17] M. Guo, P. Diao, S. Cai, J. Solid State Chem. 178 (2005) 1864.
[18] Z. Wang, B. Huang, X. Liu, X. Qin, X. Zhang, J. Wei, P. Wang, S. Yao, Q. Zhang, X. Jing, Mater. Lett. 62 (2008) 2637.
[19] Z. Wang, B. Huang, X. Qin, X. Zhang, P. Wang, J. Wei, J. Zhan, X. Jing, H. Liu, Z. Xu, H. Cheng, X. Wang, Z. Zheng, Mater. Lett. 63 (2009) 130.
[20] J.C. Johnson, H.Q. Yan, R.D. Schaller, P.B. Petersen, P.D. Yang, R.J. Saykally, Nano Lett. 2 (2002) 279.
[21] X.Q. Zhang, Z.K. Tang, M. Kawasaki, A. Ohtomo, H. Koinuma, J. Phys.: Condens. Matter 15 (2003) 5191.
[22] H. Cao, J.Y. Wu, H.C. Ong, J.Y. Dai, R.P.H. Chang, Appl. Phys. Lett. 73 (1998) 572.
[23] S.W. Chan, R. Barille, J.M. Nunzi, K.H. Tam, Y.H. Leung, W.K. Chan, A.B. Djurisic, Appl. Phys. B 84 (2006) 351.
[24] Y. Nakayama, P.J. Pauzauskie, A. Radenovic, R.M. Onorato, R.J. Saykally, J. Liphardt, P.D. Yang, Nature 447 (2007) 1098.
[25] J.H. Lin, Y.J. Chen, H.Y. Lin, W.F. Hsieh, J. Appl. Phys. 97 (2005) 033526.
[26] I.V. Kityk, A. Migalska-Zalas, J. Ebothe, A. Elchichou, M. Addou, A. Bougrine, A.Ka Chouane, Anomalously Cryst. Res. Technol. 37 (4) (2002) 340.
[27] I.V. Kityk, J. Ebothe, A. Elhichou, M. Addou, A. Bougrine, B. Sahraoui, Phys. Status Solid B 234 (2002) 553.
[28] Z. Gui, X. Wang, J. Liu, S. Yan, Y. Ding, Z. Wang, Y. Hu, J. Solid State Chem. 179 (2006) 1984.
[29] J. Ebothe, I.V. Kityk, S. Benet, B. Claudet, K.J. Plucinski, K. Ozga, Opt. Commn. 268 (2006) 269.
[30] B. Kulyk, Z. Essaidi, J. Luc, Z. Sofiani, G. Boudebs, B. Sahraoui, J. App. Phys. 102 (2007) 113113.
[31] K. Ozga, T. Kawaharamura, A. Ali Umar, M. Oyama, K. Nouneh, A. Slezak, S. Fujita, M. Piasecki, A.H. Reshak, I.V. Kityk, Nanotechnology 19 (2008) 185709.
[32] A. Douayar, M. Abd-Lefdil, K. Nouneh, P. Prieto, R. Diaz, A.O. Fedorchuk, I.V. Kityk, Appl. Phys. B 110 (2013) 419.
[33] T.M. Williams, D. Hunter, A.K. Pradhan, I.V. Kityk, Appl. Phys. Lett. 89 (2006) 043116.
[34] Feng Pan, Man Shing Wong, Martin Bosch, Christian Bosshard, Urs Meier, Peter Gunter, Appl. Phys. Lett. 71 (15) (1997) 2064.
[35] Richard L. Sutherland, Hand Book of Nonlinear Optics, second ed., Revised and Expanded–– Marcel Dekker Inc, 2003, p. 241.
[36] C.H. Hsu, D.H. Chen, Nanotechnology 21 (2010) 285603.
[37] R. Vettumperumal, S. Kalyanaraman, B. Santoshkumar, R. Thangavel, Mater. Res. Bull. 50 (2014) 7.
[38] Mohua Chakraborty, Anima Ghosh, R. Thangavel, J. Sol–Gel Sci. Technol. 74 (2015) 756.
[39] A. Douayar, A. Belayachi, M. Abd-Lefdil, K. Nouneh, Z. Laghfour, I.V. Kityk, A. Slezak, R. Miedzisnki, J. Alloys Comp. 550 (2013) 345.
[40] M.C. Larciprete, D. Haertle, A. Belardini, M. Bertolotti, F. Sarto, P. Gunter, Appl. Phys. B 82 (2006) 431.
[41] Y.R. Shen, The Principles of Nonlinear Optics, Wiley, New York, 1984.
[42] K. Geren, S.W. Liu, H.J. Zhou, Y. Zhang, R. Tian, Min Xiao, J. Appl. Phys. 105 (2009) 063531.
[43] Guan-Yu Zhuo, Kuo-Jen Hsu, Tung-Yu Su, Nan-Hsun Huang, Yang-Fang Chen, Shi- Wei Chu, J. Appl. Phys. 111 (2012) 103112.
[44] S.K. Das, M. Bock, C.O. Neill, R. Grunwald, K.M. Lee, H.W. Lee, S. Lee, F. Rotermund, Appl. Phys. Lett. 93 (2008) 181112.
[45] S.S. Kim, B.T. Lee, Thin Solid Films 446 (2004) 307.
[46] S. Kalyanaraman, R. Thangavel, R. Vettumperumal, J. Phys. Chem. Sol. 74 (2013) 504.
[47] C. Li, X.C. Li, P.X. Yan, E.M. Chong, Y. Liu, G.H. Yue, X.Y. Fan, Appl. Surf. Sci. 253 (2007) 4000.
[48] G.W. Cong, H.Y. Wei, P.F. Zhang, W.Q. Peng, J.J. Wu, X.L. Liu, C.M. Jiao, W.G. Hu, Q.S. Zhu, Z.G. Wang, Appl. Phys. Lett. 87 (2005) 231903.
[49] M.K. Kavitha, Honey John, Pramod Gopinath, Reji Philip, J. Mater. Chem. C 1 (2013) 3669.
[50] L. Castañeda, O.G. Morales-Saavedra, D.R. Acosta, A. Maldonado, M. de la L. Olvera, Phys. Stat. Sol. A 203 (8) (2006) 1971.
[51] Y.F. Li, B. Yao, Y.M. Lu, Y.Q. Gai, C.X. Cong, Z.Z. Zhang, D.X. Zhao, J.Y. Zhang, B.H. Li, D.Z. Shen, X.W. Fan, Z.K. Tang, J. Appl. Phys. 104 (2008) 083516.